J Comput Electron (2007) 6:183–186
DOI 10.1007/s10825-006-0078-6

Self-consistent quantum transport theory: Applications and assessment of approximate models

Tillmann Kubis · Peter Vogl

Published online: 9 December 2006

Abstract We have implemented a fully self-consistent nonequilibrium Green's function approach for vertical quantum transport in open quantum devices with contacts and study theoretically quantum well heterostructures, resonant tunneling diodes and quantum cascade laser structures in this formalism. We systematically investigate the role and consequences of several widely used approximations such as decoupling the equations for the scattering states and their occupation, neglect of inelastic scattering, and neglect of nonlocal scattering self-energies.

Keywords Quantum transport · NEGF · Resonant tunneling diode · Quantum cascade laser structure

1 Introduction

A realistic prediction of carrier transport in semiconductor nanoscale quantum devices requires the theory to treat multiple scattering and quantum effects such as carrier confinement, interference and capture on an equal footing. One of the most widely used methods in this context is the nonequilibrium Green's function method (NEGF) [1–3]. NEGF allows for the calculation of scattering states (represented by the retarded Green's function G^R) and their nonequilibrium occupation (represented by the lesser Green's function $G^<$). Nevertheless, it has been computationally difficult and very demanding to apply this method to resistive nanodevices where scattering is necessarily strong. Therefore, NEGF has almost always been implemented with many simplifications.

In this paper we present NEGF results for quantum well heterostructures, resonant tunneling diodes (RTD) and quantum cascade laser structures. To this end, we have implemented the NEGF formalism fully self-consistently for resistive open devices where multiple scattering is significant. We take into account acoustic and polar-optical phonon scattering as well as scattering with charged impurities, and the electron-electron scattering in Hartree approximation. Importantly, we include the full momentum and energy dependence of all phonon and impurity self-energies and employ the self-consistent Born approximation in calculating G^R, $G^<$ which is necessary to guarantee current conservation.

The primary goal of this paper is to carefully assess many of the commonly employed approximations of the NEGF formalism and, in this way, obtain insight into the reliability, accuracy, and limitations of the NEGF approach. All nanostructures in this paper are chosen to be quantum well heterostructures that are homogeneous in the lateral (x, y) directions, and to be in contact with two reservoirs at $z = 0$ and $z = L$, respectively. The electrons are described within a one-band model with a variable effective mass $m^*(z)$.

2 Decoupling of G^R and $G^<$

When we take the coupling between the lesser and the retarded Green's function fully into account, we have to solve four coupled partial differential equations (PDE). For the case of the electron-phonon interaction, these equations read

T. Kubis (✉) · P. Vogl
Walter Schottky Institute, TU München, Am Coulombwall 3,
85748 Garching, Germany
e-mail: kubis@wsi.tum.de

P. Vogl
e-mail: vogl@wsi.tum.de

in operator form

$$
\begin{aligned}
&(E - H_0 - e\Phi - \Sigma^R)G^R = 1,\\
&G^< = G^R\Sigma^< G^{R\dagger},\\
&\Sigma^< = G^< D^<,\ \Sigma^R = G^R D^R + G^R D^< + G^< D^R,
\end{aligned}
\tag{1}
$$

where H_0 is the single-electron Hamiltonian, Φ is the electrostatic potential, D denotes the phonon Green's function, and Σ denotes the self-energy. We have implemented these expressions in a real space basis so that, e.g., the self-energies $\Sigma(z, z', k_{//}, E)$ are functions of two spatial coordinates, the lateral momentum, and the energy. In this way, the scattering states, the transition probabilities between them, and their occupations are calculated self-consistently. An important role of this self-consistency is to ensure that the total scattering probability into each final state never exceeds the Pauli blocking limit. If we neglect the coupling between the scattering states (determined by G^R, Σ^R) and their occupation (determined by $G^<$, $\Sigma^<$), on the other hand, we loose this feedback mechanism and scattering events can keep filling a state beyond the Fermionic limit [4].

In order to illustrate the influence of this decoupling, Fig. 1 shows a GaAs *n-i-n* structure with an $In_{.14}Ga_{.86}$ As quantum well within the intrinsic region. The total length of the device is 50 nm with 16 nm intrinsic region embedded in between the two 17 nm *n*-regions with $n = 1 \times 10^{18}\text{cm}^{-3}$ each. Within the intrinsic region, there is a 12 nm $In_{.14}Ga_{.86}As$ quantum well of 150 meV depth. For zero applied bias, the full NEGF calculation correctly yields the equilibrium Fermi distribution $f(E) = -G^<(E)/[G^R(E) - G^{R\dagger}(E)]$ in the entire device. By contrast, the decoupled solution violates the Pauli principle as soon as any state occupancy exceeds a value of

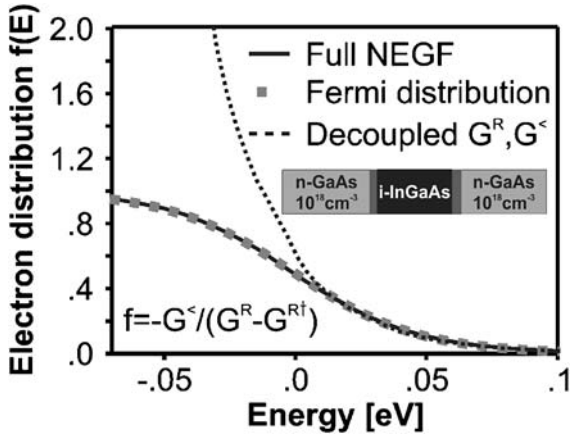

Fig. 1 Equilibrium electron distribution of a 12 nm wide GaAs/$In_{.14}Ga_{.86}As$ quantum well at 300 K calculated with fully self-consistent NEGF (full line) and with decoupled retarded and lesser Green's functions (dashed). The zero of energy is the chemical potential. The full NEGF result faithfully yields the Fermi distribution (grey dots), in contrast to the decoupled model that violates the Pauli principle

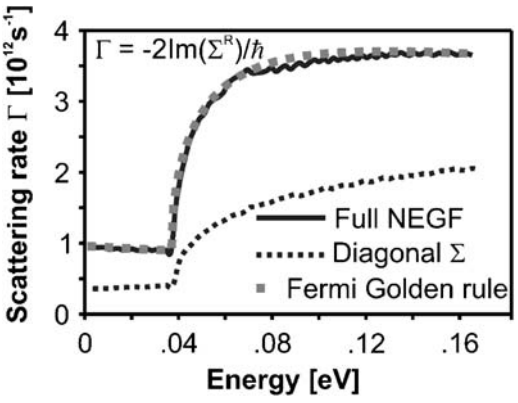

Fig. 2 On-shell scattering rate of electrons by screened polar optical phonons in homogeneous GaAs at 300 K, resulting from full NEGF calculations (full line) and with purely on-site self-energies Σ (dotted line). The scattering rate obtained from the Fermi Golden rule is shown for comparison (grey dots)

0.3. The resulting state occupation even exceeds the physical limit of 1 at energies below the chemical potential that lies at 0 eV in Fig. 1.

3 Spatially diagonal self-energies Σ

A common approximation is to assume a spatially diagonal self-energy $\Sigma(z, z', k_{//}, E) \propto \delta_{z,z'}$ [5–7]. We analyze the effect of this approximation in the case of electron scattering with polar optical phonons in homogeneous GaAs at 300 K and low carrier density $n = 1 \times 10^{16}\text{cm}^{-3}$ where the coupling between the retarded and lesser Green's functions is weak. In addition, we reduce the scattering strength by assuming a fixed screening length of 5 nm instead of 43 nm that would be consistent with the given n. In this weak-scattering limit, the imaginary part of the on-shell portion of the retarded self-energy should become identical to the lowest order scattering rate according to Fermi's Golden Rule. As we show in Fig. 2, this is indeed fulfilled in the NEGF calculation that fully includes all off-diagonal self-energies. By contrast, the scattering rate resulting from purely diagonal self-energies is significantly smaller and demonstrates the large contribution that result from non-local scattering events even for weak scattering. This result is consistent with similar findings in [7] for resonant tunneling diodes.

4 Neglect of inelastic scattering

Figure 3 shows the I-V curve of a 40 nm GaAs/$Al_{.3}Ga_{.7}As$ resonant tunneling diode with two 3 nm wide $Al_{.3}Ga_{.7}As$ barriers and a 4 nm quantum well in the center. To the left and right of the barriers, there is a 3 nm intrinsic region and a 12 nm *n*-doped region with $n = 2 \times 10^{17}\text{cm}^{-3}$,

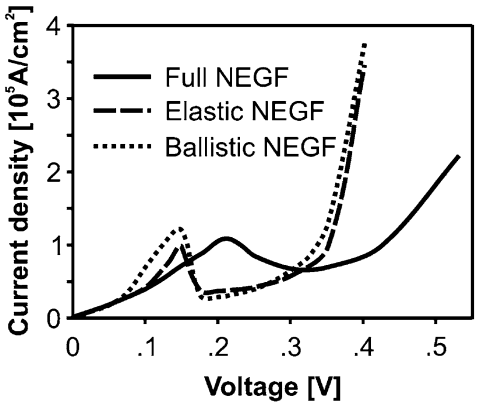

Fig. 3 Calculated current density in the GaAs/$Al_{.3}Ga_{.7}As$ resonant tunneling structure of Fig. 4 as a function of applied bias. The full NEGF calculations (full line) are compared with approximate models that invoke solely elastic scattering (dashed) or no incoherent scattering at all (dotted)

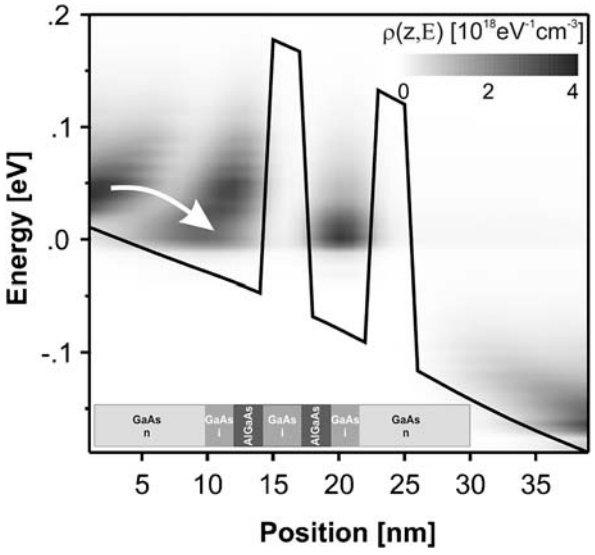

Fig. 4 Conduction band profile of GaAs/$Al_{.3}Ga_{.7}As$ resonant tunneling structure as described in the text, plotted at the resonant bias voltage of 200 mV. The energy resolved electron density is shown as contour plot. The arrow is meant to guide the eye and shows the trapping of electrons into the triangular quasi-bound state in front of the barriers

respectively. Figure 3 shows a comparison of the full NEGF calculation (···) with a ballistic calculation (—) and a simplified model (—) that neglects all inelastic and off-diagonal phonon scattering processes ($\Sigma(z, z') \propto \delta_{z,z'}$) at 300 K. Computationally, the latter two approaches are orders of magnitudes faster. However, inelastic scattering is required to occupy the triangular quasi-bound state that forms in front of the left barrier of any RTD under forward bias (see Fig. 4). This state acts as feeding mechanism for the RTD; in fact, the peak current occurs at a bias voltage where this quasi-bound state is aligned with the resonant quantum well state [8]. This is illustrated in Fig. 4 that depicts the potential profile and the energy resolved electron density, defined by

$$\rho(z, E) = \frac{2}{(2\pi)^3}\mathrm{Im}\int d^2k_{//}G^{<}(z, z, k_{//}, E) \quad (2)$$

at the resonant bias voltage of 200 mV. Note that the electrons that drift out of the contact first loose energy before they traverse the resonance state in the well. If we neglect inelastic scattering or even any kind of scattering (i.e. assume ballistic transport) [9], the RTD functions in an entirely different way. The electrons in the contact fly towards the barrier, maintaining their (high) energy and therefore hit the resonance energy in the well at a significantly lower bias. The I-V characteristic is then entirely determined by the properties of the contact rather than by the doping of the device. A careful inclusion of all inelastic processes is therefore necessary to capture the physical mechanisms that determine the resonance bias and peak value of the RTD.

5 Quantum cascade laser structure

In Fig. 5, we show the results of a full NEGF calculation of the potential profile and the energy resolved electron density in the active region of a GaAs/$Al_{.15}Ga_{.85}As$ quantum cascade laser structure. The geometry and doping of the structure has been taken from [10]. The results illustrate the necessity to treat coherent and incoherent quantum transport on an equal footing. The inverted occupation of the two resonance levels in the central double quantum well is clearly visible. The calculated photon emission energy is 17.0 meV which agrees very well with the experimental value of 14.2 meV

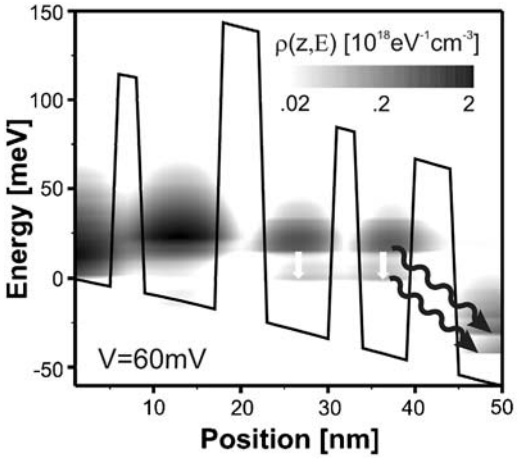

Fig. 5 Conduction band profile of 50 nm GaAs/$Al_{.15}Ga_{.85}As$ quantum cascade laser structure from Ref. [10] at a bias voltage of 60 mV and at 100 K. The energy resolved electron density is shown as contour plot. The arrows are only meant to guide the eye and show the calculated emission energies (white = photons, black = phonons)

[10]. The inelastic LO phonon (of 35 meV energy) emission process across the last barrier on the right hand side efficiently empties the lower of the double quantum well levels, also in accord with the data. We note that the largely coherent tunneling from the leftmost well into the rightmost well leads to a population inversion already for voltages that are lower than the resonance condition which is obtained at 60 mV in the present case.

6 Conclusion

In summary, we have analyzed the vertical carrier transport through several quantum devices employing a fully implemented NEGF formalism. We have assessed several commonly employed approximations and find off-diagonal self-energies to substantially affect the optical phonon scattering rate. The coupling between the retarded and lesser Green's functions has been shown to be a prerequisite for obtaining the correct carrier occupation in the equilibrium limit. A study of RTD's has revealed that inelastic scattering plays a vital role in determining the resonance condition for the current. Financial Support by the Österreichische FWF (Projekt IR-ON F025) and Deutsche Forschungsgemeinschaft (SFB 631) is gratefully acknowledged.

References

1. Datta, S.: Electronic Transport in Mesoscopic Systems. Cambridge University Press (1995)
2. Ferry, D.K., Goodnick, S.M.: Transport in Nanostructures. Cambridge University Press (1997)
3. Schäfer, W., Wegener, M.: Semiconductor Optics and Transport Phenomena. Springer (2002)
4. Lake, R., Klimeck, G., Bowen, R.C., Jevanovic, D.: Single and multiband modeling of quantum electron transport through layered semiconductor devices. J. Appl. Phys. **81**, 7845 (1997)
5. Wacker, A.: Semiconductor superlattices: a model system for nonlinear transport. Phys. Rep. **357**, 1–111 (2002)
6. Venugopal, R., Paulsson, M., Goasguen S., Datta, S., Lundstrom, M.: A simple quantum mechanical treatment of scattering in nanoscale transistors. J. Appl. Phys. **93**, 5613 (2003)
7. Klimeck, G., Lake, R., Fernando, C.L., Bowen, R.C., Blanks, D., Leng, M., Moise, T., Kao Y.C., Frensley, W.R.: Numerical approximations for polar optical phonon scattering in resonant tunneling diodes. In: Ismail, K., Bandyopadhyay, S., Leburton, J.P. (eds.) Quantum Devices and Circuits. Imperial Press, London (1996)
8. Fischetti, M.V.: Theory of electron transport in small semiconductor devices using the Pauli master equation. J. Appl. Phys. **83**, 270 (1998)
9. Laux, S.E., Kumar, A., Fischetti, M.V.: Analysis of quantum ballistic electron transport in ultrasmall silicon devices including space-charge and geometric effects. J. Appl. Phys. **95**, 5545 (2004)
10. Williams, B.S., Callebaut, H., Kumar, S., Hu, Q., Reno, J.: 3.4-THz quantum cascade laser based on longitudinal-optical phonon scattering for depopulation. Appl. Phys. Lett. **82**, 1015 (2003)